

Output-only computer vision based damage detection using phase-based optical flow and unscented Kalman filters



Y.-J. Cha^{a,*,1}, J.G. Chen^b, O. Büyüköztürk^c

^a Department of Civil Engineering, University of Manitoba, Winnipeg MB R3T 5V6, Canada

^b Department of Civil and Environmental Engineering, Massachusetts Institute of Technology, Cambridge, MA 02139, USA

^c Laboratory for Infrastructure Science and Sustainability (LISS), Department of Civil and Environmental Engineering, Massachusetts Institute of Technology, Cambridge, MA 02139, USA

ARTICLE INFO

Article history:

Received 4 May 2016

Revised 16 November 2016

Accepted 17 November 2016

Keywords:

Motion magnification

Phase-based optical flow

Video

Computer vision

Non-contact measurement

System identification

Unscented Kalman filters

ABSTRACT

A damage detection methodology is proposed by integrating a nonlinear recursive filter and a non-contact computer vision based algorithm to measure structural dynamic responses. A phase-based optical flow algorithm inspired by the motion magnification technique is used to measure structural displacements, and the unscented Kalman filter is used to predict structural properties such as stiffness and damping coefficients. This non-contact displacement measurement methodology does not require an intensive instrumentation process, does not add any additional mass to the structure which may skew measurements, and can measure more signals compared to traditional methods. This measurement methodology still needs improvement as a tool due to its higher noise level relative to traditional accelerometer and laser vibrometer measurements. In order to detect structural damage using measured displacements from video, an unscented Kalman filter is used to remove noise from the displacement measurement and simultaneously detect damage by identifying the current stiffness and damping coefficient values, given a known mass, which are used to detect damage. To validate the proposed damage detection method state-space equations are derived without external excitation input and experimental tests are carried out. The experimental results show reasonable and accurate predictions of the stiffness and damping properties compared to dynamic analysis calculations.

© 2016 Elsevier Ltd. All rights reserved.

1. Introduction

The deterioration of mechanical systems and accelerated deterioration of infrastructure due to an increasing number of vehicles and people has led to a rising interest in the safety and monitoring of mechanical systems and infrastructure. In order to evaluate the safety of structural systems or detect damage, the measured dynamic response of structures using accelerometers has been widely used [1]. In terms of predicting a structure's nonlinear behavior, displacement inherently contains more information on dynamic behavior than the structure's acceleration or velocity responses. The displacement response is typically measured by linear variable-differential transformers (LVDT) and global positioning system (GPS) receivers. LVDT is a contact based measurement tool requires a separate stationary platform as a measurement reference that the sensor is fastened to, which can be impractical. GPS

has a multi-path issue as a major source of error, especially in urban environments and has worse displacement and time resolution compared to other approaches.

Digital camera based direct displacement measurement approaches have been proposed to overcome the disadvantages of contact based LVDT and GPS based measurements [2–3]. Wahbeh et al. [4] presented an analytical and experimental study on the feasibility of a vision-based approach for obtaining direct measurements of the absolute displacement time history at select locations of a structure. Lee and Shinozuka [5] also developed a dynamic displacement system using digital image processing techniques, which showed reliable agreement with a laser vibrometer.

Recently, Chen et al. [6] developed a methodology in which phase-based optical flow was used to measure displacements in videos. This non-contact approach provides the capability to remotely monitor and inspect structural systems because of the commonplace availability, simplicity, and potential low cost of video cameras. Due to its non-invasive approach, it is also applicable to small mechanical systems and many points can be measured using one video measurement. This video camera based method also

* Corresponding author.

E-mail address: young.cha@umanitoba.ca (Y.-J. Cha).

¹ Formerly, Massachusetts Institute of Technology, Cambridge, MA, USA.

provides the unique capability of collecting high density spatial data. The measured displacement is accurate when compared to the displacement signal determined from post-processing of a velocity or acceleration signal measured from a laser vibrometer or accelerometer, however it suffers from higher levels of noise. The experimental tests conducted showed that the camera had a noise floor several orders of magnitude worse than the laser vibrometer and accelerometer. To remedy this, a filtering method could be used to remove noise from measured data, to predict structural responses where sensors are not installed, and to identify the structural system.

Sophisticated computational methods such as least-squares estimation and Kalman filtering have been applied to identify changes in system properties and remove noise in measured data; these methods have also been applied to damage detection problems for civil structures. Based on least-squares estimation (LSE), adaptive tracking techniques were proposed to identify the time-varying system parameters of linear and nonlinear structures [7–9]. Hoshiya and Saito [10] applied an extended Kalman filter (EKF) to the system identification problem of seismic structural systems. A weighted global iteration procedure with an objective function has been incorporated into the EKF algorithm to achieve a stable prediction. The advantage of the EKF compared to LSE is that it provides more accurate results by removing numerical integrations to get velocity or displacement responses. In order to improve the EKF, Yang et al. [11] followed by proposing an adaptive EKF to identify changes in the linear and nonlinear system parameters using the constrained optimization algorithm. The unscented Kalman filter (UKF), originally developed by Julier et al. [12] and Julier and Uhlmann [13] has also been used in nonlinear system identification by Wu and Smyth [14] and Chatzi and Smyth [15]. This approach uses structural vibration measurements and input excitation measurements, and shows superior performance compared to the EKF-based approaches. UKF uses carefully chosen points (i.e., sigma points) to represent the state which is approximated by a Gaussian random variable (GRV). This approach does not require calculation of Jacobians, which introduce large errors in the true posterior mean and covariance of the transformed GRV of the error to linearize the state equations. This quasi-real-time method of detecting damage can contribute to reducing the socio-economic burden because it can detect damage at early stages that may not necessitate closing bridges, thus avoiding traffic jams. Many researches have been carried out using UKF or its enhanced version to identify structural systems [16–18]. Thus, in this paper, UKF is used as a nonlinear system identification method with the input of the displacement signals calculated from a video by a method related to phase-based optical flow processing.

2. Purpose and concept

The objective of this paper is to propose a non-contact measurement based damage detection method by integrating a computer vision method using phase-based optical flow processing and unscented Kalman filter, and demonstrate its performance. The formulation for the calculation of displacement of moving objects in videos from optical flow is introduced. State-space equations without external excitation input are developed for use with the unscented Kalman filter which is used to reduce measurement noise and predict structural properties such as stiffness and damping coefficients as a basis for system identification and damage detection. An experimental study is carried out on cantilever beams with separate intact, notched, and reduced-section beams as well as with loosened support bolts as damage cases to validate the proposed damage detection method.

A schematic view of the proposed approach is shown in Fig. 1. A video is first collected using a camera from a structure of interest. Using the time series of images, a phase-based optical flow process is applied to calculate absolute displacements of points on the structure with good contrast. The extracted displacement is used as a measured input to the UKF to predict system states including the structural properties which can then be used to determine whether or not the structure is damaged compared to intact structural measurements.

3. Theory and methods

The proposed damage detection method uses displacement signals from a video as an input to the unscented Kalman filter to predict system states including stiffness and damping. In this section the phase-based optical flow process is described as a method to calculate displacement signal from a video, as well as the details of an unscented Kalman filter (UKF) as a system identification method and dynamic equation of the motion to establish the state-space equation without excitation input.

3.1. Phase-based motion magnification for displacement extraction from video

Chen et al. [6] proposed a displacement measurement methodology from video, inspired by phase-based motion magnification [19]. The fundamental concept is a phase-based approach to estimate the optical flow field using a technique similar to that developed by Wadhwa et al. [19]. In order to calculate displacement, the signal of a video is decomposed by complex spatial filters [20] into the local spatial phase and amplitude. The decomposed local phase and amplitude are used to calculate the displacement signal and edge strength simultaneously [21,22]. The relationship between local amplitude and phase and image brightness specified by $I(x, y, t)$ at spatial location (x, y) and time t is [6]:

$$A_{\theta}(x, y, t_0)e^{i\phi_{\theta}(x, y, t_0)} = (G_2^{\theta} + iH_2^{\theta}) \otimes I(x, y, t_0) \quad (1)$$

where $A_{\theta}(x, y, t_0)$ is the local amplitude, $\phi_{\theta}(x, y, t_0)$ is the local phase, and $G_2^{\theta} + iH_2^{\theta}$ is a convolution kernel of a quadrature pair filter that differs in phase by 90° . The details of the kernel are shown in the Appendix [20]. Table A1 shows convolution kernels representing a quadrature pair that differs in phase by 90° for processing the video frame. Fig. A1 shows the filters used to compute the local phase and the amplitude. The images represent a 9×9 grid of numbers in which the gray level corresponds to the value of the filter, which is given explicitly in Table A1. More information is available in Chen et al. [6]. The local phase and amplitude in orientation θ at a frame at time t_0 are computed by spatially bandpassing the frame with the complex filter. The video sequence is downsampled by a factor of 2 in each dimension spatially prior to application of the filters for ease of processing. Constant contours of the local phase through time correspond to the displacement signal which can be expressed as

$$\phi_{\theta}(x, y, t_0) = c \quad (2)$$

for some constant c [21,22]. Differentiating with respect to time yields

$$\left(\frac{\partial \phi_{\theta}(x, y, t)}{\partial x}, \frac{\partial \phi_{\theta}(x, y, t)}{\partial y}, \frac{\partial \phi_{\theta}(x, y, t)}{\partial t} \right) \cdot (u, v, 1) = 0 \quad (3)$$

where u, v are the velocity in the x and y directions respectively. Only the x direction is calculated for the purposes of this paper and the orientation θ of the filter is along the horizontal direction. Thus, the velocity in pixel units are

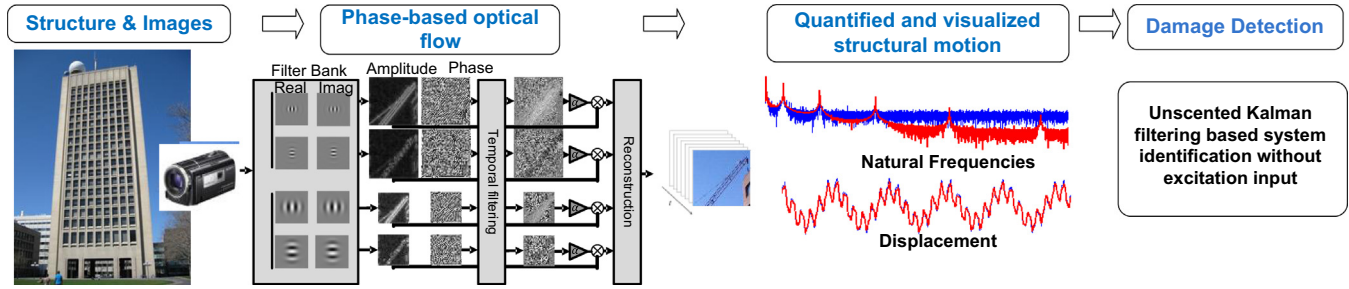


Fig. 1. Schematic view of the video based damage detection system.

$$u = -\left(\frac{\partial\phi_0(x,y,t)}{\partial x}\right)^{-1} \frac{\partial\phi_0(x,y,t)}{\partial t} \quad (4)$$

In order to compute a displacement signal in time, the velocity u in Eq. (4) between the i th frame and the first frame for all frames i are calculated. The signal to noise ratio of the displacement signal is increased by calculating a local weighted average of the displacement signal weighted by edge strength. The calculated displacement signal is converted to units of millimeters by multiplying the ratio of the length of an object in the scene divided by the number of pixels it spans.

Displacement signals can be calculated everywhere on a structure with well-defined edges using this technique. Determining the motion in textureless regions is an open problem in computer vision known as dense optical flow [23,24]. For practical purposes for measuring structures, in areas without edges or texture, edges can be added by artificial marking using tape or paint to measure displacements in that location.

The displacement signal from camera measurement has more noise than other measurement tools such as a laser vibrometer and accelerometer from the noise comparative experimental tests by Chen et al. [6]. The discrepancy in correlation between the camera and laser vibrometer displacement signals is 0.04%. The noise floor of the camera was approximately 1×10^{-5} pixels per root Hertz from given conversion factor of 480 pixels for 104 mm.

3.2. Unscented Kalman filtering

In order to remove measurement noise from the video derived displacements and to predict structural properties such as stiffness and damping, the unscented Kalman filter is used. Consider the general dynamic nonlinear discrete time system,

$$x_k = f(x_{k-1}, w_{k-1}) \quad (5)$$

$$z_k = h(x_k, v_k) \quad (6)$$

where x_k is the state variable vector at time step k , and w_k and v_k are Gaussian random white noise with covariance matrices Q_k and R_k , and z_k is the observation vector. The fundamental procedure of the UKF is prediction and calculation of the Kalman gain and estimation, which is similar to the procedure of the traditional linear Kalman filter and EKF to determine the minimum-mean squared error estimate of the state vector of the nonlinear discrete time system. The difference is that the state is approximated by GRV represented by a set of sigma points as described in the introduction. Let us consider system state x_k , in which the mean is x_{km} and covariance is P_{xk} .

$$x_k = N(x_{km}, P_{xk}) \quad (7)$$

Markov chain based iterative UKF procedures start by defining initial values of the estimated system parameters:

$$\hat{x}_0 = E(x_0), \quad P_{x0} = E[(x_0 - \hat{x}_0)(x_0 - \hat{x}_0)^T] \quad (8)$$

where \hat{x}_0 is initial estimated state and P_{x0} is covariance. From the states, sigma points χ_i and weights W_i are calculated using a Cholesky decomposition condition,

$$(\chi_i, W_i) \leftarrow (\hat{x}_{k-1}, P_{xk-1}, \kappa) \quad (9)$$

$$\chi_1 = \hat{x}_{k-1}, \quad \chi_{i+1} = \hat{x}_{k-1} + u_i, \quad \text{and} \quad \chi_{i+n+1} = \hat{x}_{k-1} - u_i \quad (10)$$

$$W_1 = \frac{\kappa}{n + \kappa}, \quad W_{i+1} = \frac{\kappa}{2(n + \kappa)}, \quad \text{and} \quad W_{i+n+1} = \frac{\kappa}{2(n + \kappa)} \quad (11)$$

where n is number of parameters, $i = 1, 2, \dots, n$, κ is generally defined to satisfy $n + \kappa = 3$, and u_i is the row vector of the matrix U , satisfying the following Cholesky decomposition condition:

$$U^T U = (n + \kappa) P_{xk} \quad (12)$$

Predicted system parameters, \hat{x}_k^- , and posterior covariance, P_{xk}^- , in Eq. (13), and measured parameters, \hat{z}_k^- , and its error covariance, P_{zk}^- , are estimated in Eq. (14) using sigma points and weights, and Kalman gain, K_k , is estimated in Eq. (15). These procedures are as expressed in Fig. 2:

$$\begin{aligned} \hat{x}_k^- &= \sum_{i=1}^{2n+1} W_i f(\chi_i), \quad P_{xk}^- \\ &= \sum_{i=1}^{2n+1} W_i \{f(\chi_i) - \hat{x}_k^-\} \{f(\chi_i) - \hat{x}_k^-\}^T + Q_k \end{aligned} \quad (13)$$

$$\begin{aligned} \hat{z}_k^- &= \sum_{i=1}^{2n+1} W_i h(\chi_i), \quad P_{zk}^- \\ &= \sum_{i=1}^{2n+1} W_i \{h(\chi_i) - \hat{z}_k^-\} \{h(\chi_i) - \hat{z}_k^-\}^T + R_k \end{aligned} \quad (14)$$

$$P_{xz} = \sum_{i=1}^{2n+1} W_i \{f(\chi_i) - \hat{x}_k^-\} \{h(\chi_i) - \hat{z}_k^-\}^T, \quad K_k = P_{xz} P_{zk}^{-1} \quad (15)$$

System parameters, \hat{x}_k , are updated using measured states of the system, z_k , and error covariance, P_{xk} , is calculated using Kalman gain:

$$\hat{x}_k = \hat{x}_k^- + K_k (z_k - \hat{z}_k^-) \quad (16)$$

$$P_{xk} = P_{xk}^- - K_k P_{zk}^- K_k^T \quad (17)$$

where the time step k is incremented. The \hat{x}_k in Eq. (16) is predicted states of the dynamic system.

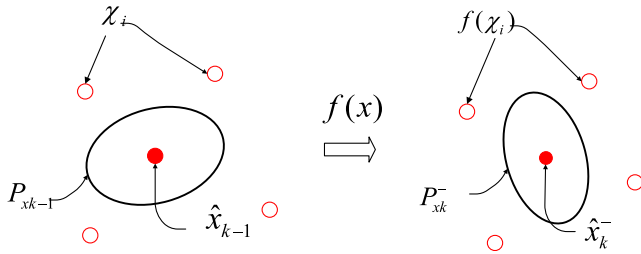


Fig. 2. Transformation of the sigma points.

3.3. Dynamic equations of motion for cantilever beam excited by impact force

In order to apply UKF to predict states including stiffness and damping coefficients, dynamic equation of motion is required to establish state space equation (Eq. (5)). The dynamic equation of a single-degree-of-freedom system (SDOF) excited by impact force is,

$$M\ddot{x} + C\dot{x} + Kx = F_e(t) \quad (18)$$

where M is mass, C is damping coefficient, K is stiffness, and F_e is impact force input. The displacement response is derived by considering impact force application at a time, a and assuming there is no other excitation input to the SDOF system is as follows,

$$x(t) = x(a)e^{-\zeta\omega_n(t-a)} \cos \omega_d(t-a) + \left\{ \frac{\zeta\omega_n x(a) + \dot{x}(a)}{\omega_n \sqrt{1-\zeta^2}} \right\} e^{-\zeta\omega_n(t-a)} \sin \omega_d(t-a) \quad (19)$$

where the critical damping ratio and undamped and damped natural frequencies are defined as $2\zeta\omega_n = C/M$, $\omega_n = \sqrt{K/M}$, and $\omega_d = \omega_n \sqrt{1-\zeta^2}$ due to usual critical damping ratio range of 2–10% (i.e., $0.02 \leq \zeta \leq 0.10$) for civil structures. Eq. (19) is used to establish the state space equation in Eq. (5) for unscented Kalman filtering. These state space equations are as follows:

$$f(x) = \begin{bmatrix} x_{1(k+1)} \\ x_{2(k+1)} \\ x_{3(k+1)} \\ x_{4(k+1)} \\ x_{5(k+1)} \end{bmatrix} = \begin{bmatrix} x_{4(k)} e^{-\zeta\omega_n(k-a)} \cos \omega_d(k-a) + \left\{ \frac{\zeta\omega_n x_{4(k)} + x_{5(k)}}{\omega_n \sqrt{1-\zeta^2}} \right\} e^{-\zeta\omega_n(k-a)} \sin \omega_d(k-a) \\ x_{2(k)} \\ x_{3(k)} \\ x_{4(k)} \\ x_{5(k)} \end{bmatrix} \quad (20)$$

$$h(x) = [z_{1(k+1)}] = \left[x_{4(k)} e^{-\zeta\omega_n(k-a)} \cos \omega_d(k-a) + \left\{ \frac{\zeta\omega_n x_{4(k)} + x_{5(k)}}{\omega_n \sqrt{1-\zeta^2}} \right\} e^{-\zeta\omega_n(k-a)} \sin \omega_d(k-a) \right] \quad (21)$$

where $x = [x_1 \ x_2 \ x_3 \ x_4 \ x_5]^T = [x \ K \ C \ x(a) \ \dot{x}(a)]^T$, i.e., $x_{1(k)}$ is displacement, $x_{2(k)}$ is stiffness, $x_{3(k)}$ is damping, $x_{4(k)}$ is displacement at the moment, a , of impact, and $x_{5(k)}$ is velocity at the moment of impact. All ζ , ω_n , and ω_d in Eqs. (20) and (21) are

expressed as state-space variables for UKF process. The $x(a)$ and $\dot{x}(a)$ are displacement and velocity at the time (a) of impact. These two variables are included as states which should be predicted by the UKF because the governing dynamic equation of the motion at time greater than a after an impact excitation as expressed in Eq. (19) include these values, and these values are difficult to calculate based on the measurement.

4. Experiments

The proposed damage detection method is demonstrated through experimental tests. The details of the experimental setup, damage scenarios and their case studies are described in this section.

4.1. Experimental setup for case studies

Various steel cantilever beams are used as experimental structures to validate the proposed damage detection method. The experimental setup is presented in Fig. 3. The Phantom v10 model is used as a video camera [25]. There is no specific filter applied, and two normal camera lights are installed to obtain proper brightness. The video resolution and frame rate are 200×1248 and 2000 fps, respectively. The steel cantilever beams are excited by an impact hammer and the displacement response at the free end of the beam is calculated from the measured video as previously described. The distance between the video camera and cantilever beam is about 2 m.

4.2. Damage scenarios

Three different cantilever beams are used: intact beam, notched damage beam, and section-reduced beam as types of member damage as shown in Fig. 4. They are attached to a massive concrete base by four bolts. Each beam has four different connection damage scenarios: no bolts loosened, one bolt loosened, two bolts loosened, and three bolts loosened as shown in Fig. 5. Intact and notched damage steel cantilever beam sections are 0.00635 m by 0.0508 m with a length of 0.6096 m. The section-reduced beam has a reduced width

of 0.023 m in the middle of the beam. Nominal values for the Young's modulus of the steel is 1.96E11 N/m² and density is 7800 kg/m³, while the measured mass of each beam is 1.6438 kg, 1.6418 kg, and 1.168 kg for the intact, notched, and section-reduced beam, respectively.

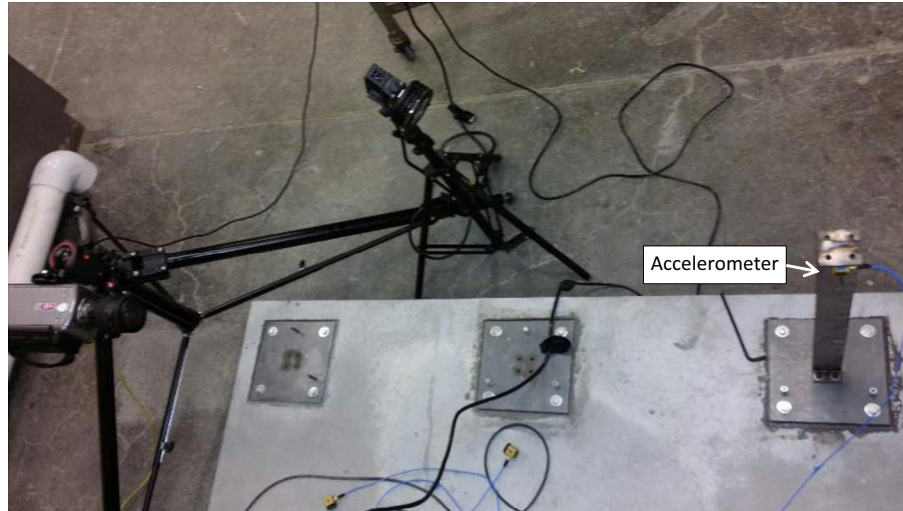


Fig. 3. Experimental setup involving a video camera and steel cantilever column.

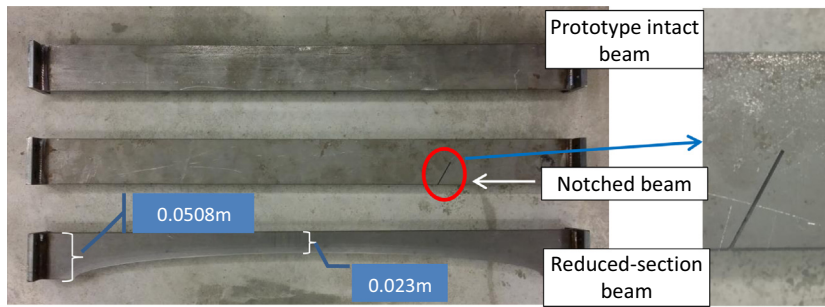


Fig. 4. Intact, notched damage, and section-reduced steel beams.

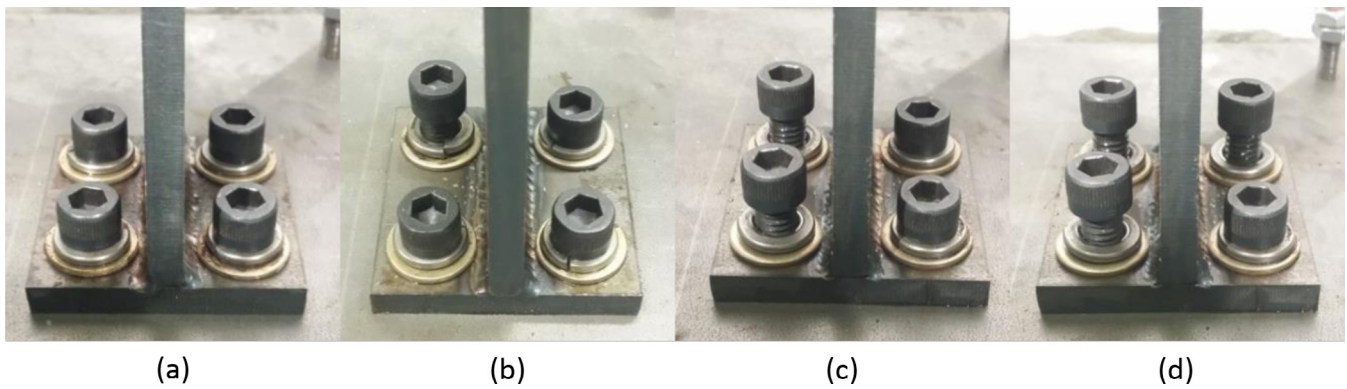


Fig. 5. Bolt loosening connection damage scenarios (a) intact (no bolts loosened), (b) one bolt loosened, (c) two bolts loosened, (d) three bolts loosened.

Table 1
Initial conditions of state parameters of the SDOF model and calculated values.

State parameters	Hand calculations	Initial conditions	Units
$x(0)$	0	0	m
$\dot{x}(0)$	0	0	m/s
$x(a)$	N/A	0	m
$\dot{x}(a)$	N/A	0	m/s
M	$0.411^a/0.3030^b$	$0.411^a/0.3030^b$	kg
$K(0)$	2813.5	2000	N/m
$C(0)$	0.0871	0.01	N s/m

^a Intact beam.

^b Reduced-section beam.

4.3. Experimental case studies

The initial estimates of the state space variables do not need to be close to the true values because the UKF can recursively correct the predicted values to produce accurate values. For Kalman filtering of intact cantilever beam, the initial values of the variables of the governing equation of the motion are presented in Table 1. The measured mass values of the intact, notched, and section-reduced cantilever beams are used to define the initial values of the masses for each UKF analysis. The initial masses are calculated based on equivalent mass which is $0.227 M_t$. M_t is the total mass of the cantilever beam including the weights of flange and sensor. The equivalent stiffness value of the intact beam is calculated using

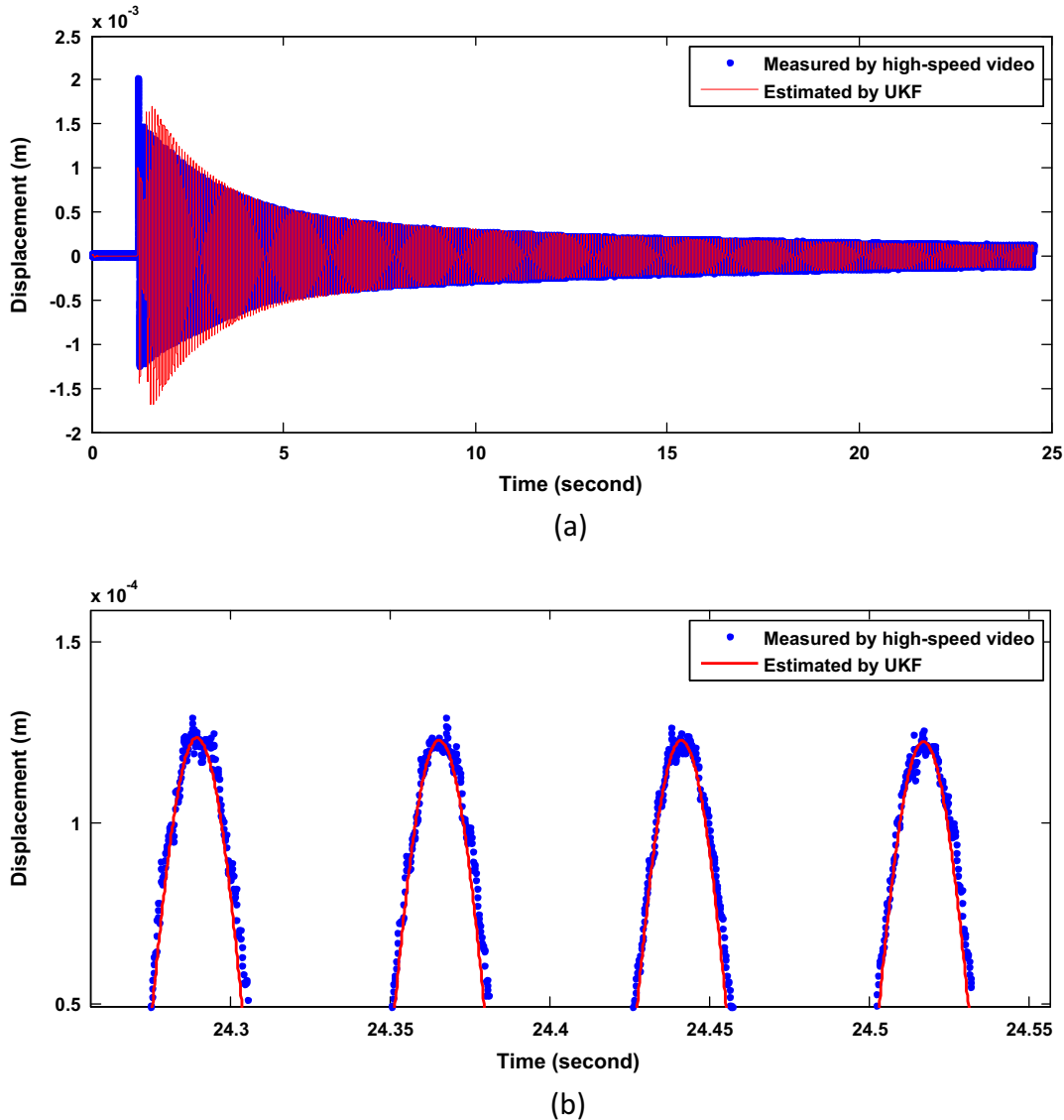


Fig. 6. Intact beam; (a) displacement comparison between measured by phase-based optical flow and predicted by UKF; (b) detailed view of the displacement comparison.

$K(0) = 3EI/L^3$ where E , I , and L are Young's modulus, second moment of inertia, and length of the beam, respectively. The damping coefficient is calculated using the measured displacement time history. Three different cantilever beams with four different bolts loosened scenarios are tested to demonstrate the performances of the proposed method to identify structural states and detect damages eventually.

4.3.1. Case 1: Intact cantilever beam

The intact cantilever beam was tested with three different connection damage levels by loosening the bolts connecting it to the concrete base. For the Kalman filtering process, tuned measurement and process noise covariances determined by trial and error are used as $9E - 6$, and $3.16E - 8I_5$, respectively. The initial selection of the error covariance P_{00} only effects the convergence speed, and the values are defined by trial and error as $P_{00} = \text{diag}[10^{-1} \ 10^4 \ 10^{-1} \ 10^{-1} \ 10^{-1}]$ for the damage scenario cases of all three beams.

The noises from displacement measurement using motion magnification algorithms for use with video are clearly removed when using the UKF. Fig. 6(a) shows the comparison between the

measured displacement from video and the predicted displacement from the UKF and Fig. 6(b) shows a detailed view. There is a discrepancy between measured displacement and predicted displacement in the initial impact because UKF requires time to predict the responses without excitation inputs. However, overall, the two responses show good agreement. Based on this fact, the UKF predicted stiffness values of the intact cantilever beam in four different cases of loosened bolts, as shown in Fig. 7. From the 24.532 s video, the displacements are measured from and used as an input to the UKF procedure.

The predicted stiffness value (i.e., 2815.5 N/m) of the intact with no bolts loosened case is nearly exactly the same as the hand calculated stiffness value (2813.5 N/m) of the intact beam. The predicted stiffness values are gradually lower from the one bolt loosened case to the three bolts loosened case as shown in Fig. 7 (a). Meanwhile, the damping coefficients increased with increasing numbers of bolts loosened as shown in Fig. 7(b) with a detailed view. In Table 2, all the predicted and calculated stiffness and damping coefficients from UKF and dynamic analysis calculations are compared. The stiffness and damping coefficients are calculated from the displacement measurements by calculating the critical damping ratio, ζ , using $\zeta = 1/(2\pi n) \log(\text{peak1}/\text{peak2})$ where n

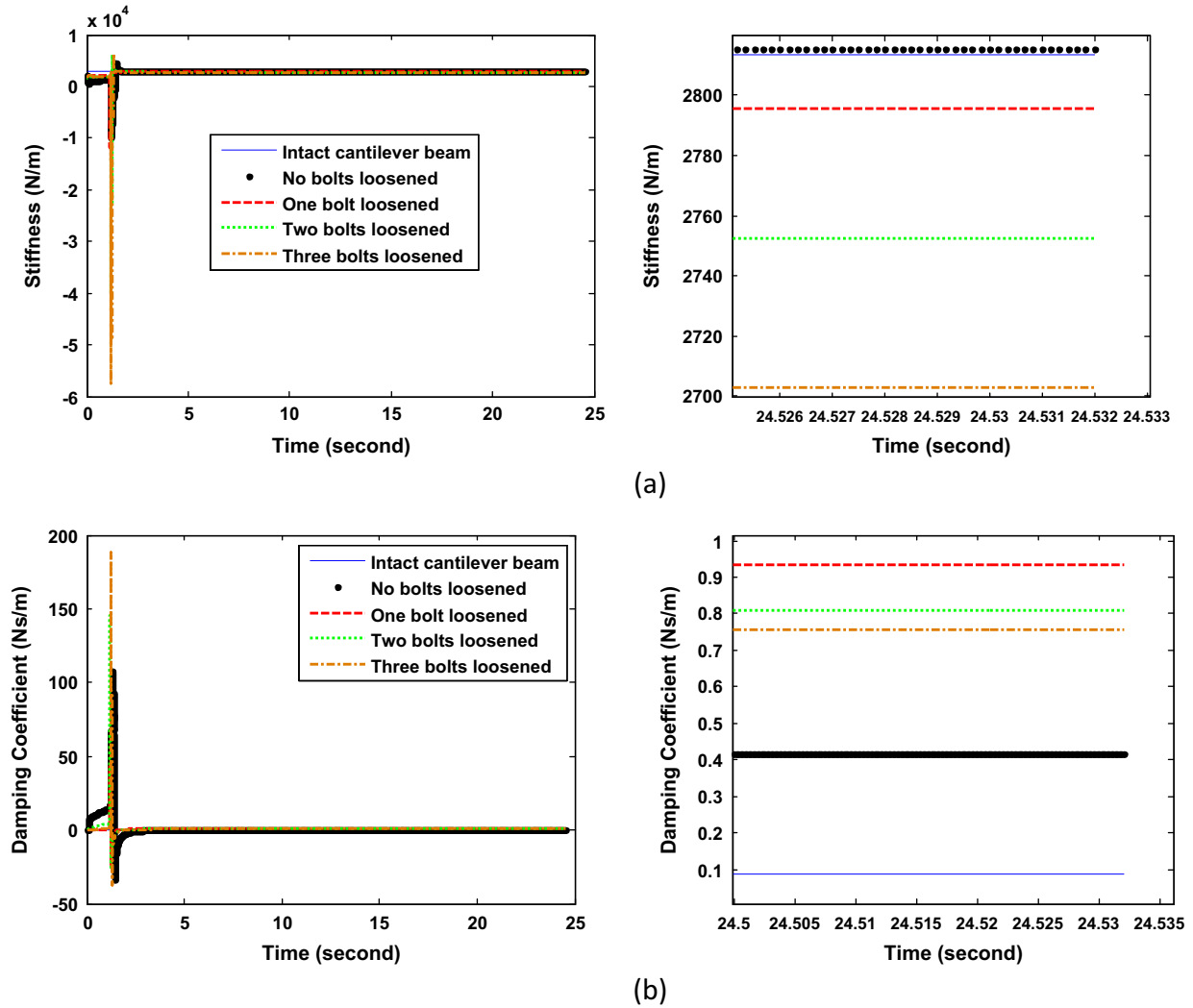


Fig. 7. Intact beam; (a) detailed view of predicted stiffness values of the intact beam with bolts loosened scenarios; (b) detailed view of predicted damping coefficients of the intact beam with bolts loosened scenarios.

Table 2

UKF predicted and calculated stiffness and damping coefficients of intact beam cases.

		No bolts loosened	One bolt loosened	Two bolts loosened	Three bolts loosened
Stiffness (N/m)	UKF predicted	2815.5	2795.4	2752.4	2702.7
	Calculated	2813.5	2794.8	2721.5	2714.8
Damping coefficient (N s/m)	UKF predicted	0.4183	0.9354	0.8084	0.7584
	Calculated	0.0871	0.0830	0.0978	0.0913

is number of sinusoidal circles and $peak1$ is first peak and $peak2$ is last peak of the sinusoidal circle. And stiffness values are calculated using $K = (2\pi f_n)^2 M$, and $C = 2\zeta\sqrt{KM}$. There are small discrepancies (i.e., approximately 1.4%) between the predicted and calculated stiffness values from the measured displacement. Regarding the damping coefficient values, even though the predicted damping values by UKF are approximately 5–15 times larger than the calculated values from displacement measurements, the predicted values are still in the reasonable range because the critical damping ratio, ζ , is 0.0138 calculated from $C = 2\zeta\sqrt{KM}$, that is smaller than 2% damping ratio for steel structures.

4.3.2. Case 2: Notched cantilever beam

In order to investigate the change in stiffness and damping due to small damage in the beam, a notched cantilever beam was

manufactured and tested with the same connection damage scenarios caused by loosening bolts. Fig. 8(a) shows the reduction of the stiffness due to the notch in the cantilever beam with and without bolts loosened. Fig. 8(b) shows the changes in the damping coefficients due to the same damage scenarios and their detailed view. Due to the notch, the predicted stiffness value of the cantilever beam is reduced from 2815.5 N/m to 2626.5 N/m which represents approximately a 7% reduction. This predicted stiffness is quite reasonable compared to the results (i.e., 2626.5 N/m) of a FE analysis using the commercial software ABAQUS [26]. The calculated damping coefficient of the notched cantilever beam from the measured displacement increased from 0.0871 N s/m in the intact beam to 0.0894 N s/m. All the structural properties predicted by UKF using different the connection damage scenarios are presented in Table 3. The predicted stiffness values of the notched

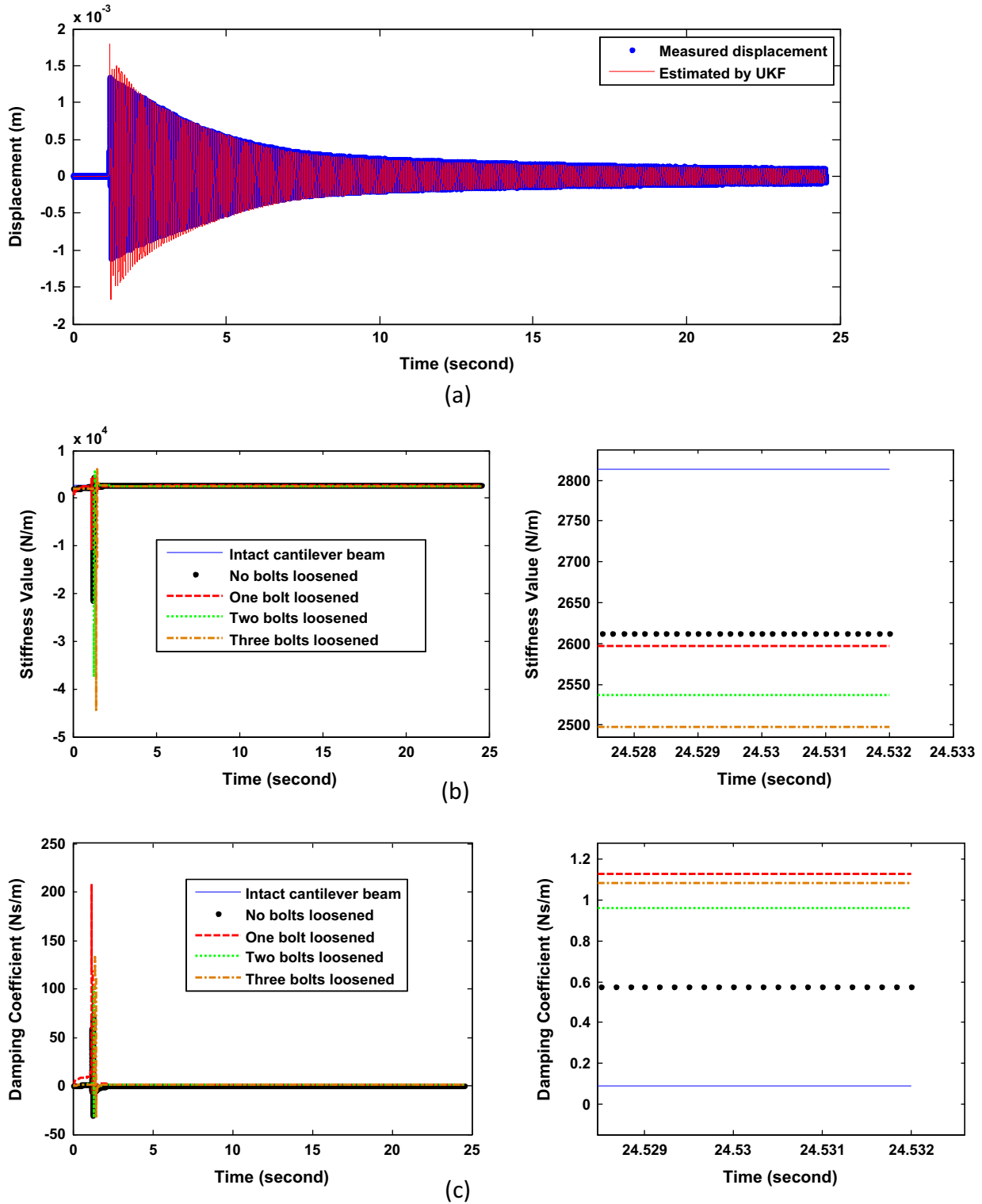


Fig. 8. Notched beam; (a) displacement comparison between measured by phase-based optical flow and predicted by UKF; (b) detailed view of predicted stiffness values of the notched beam with bolts loosened scenarios; (c) detailed view of predicted damping coefficients of the notched beam with bolts loosened scenarios.

Table 3
UKF predicted and calculated stiffness and damping coefficients of notched beam cases.

		No bolts loosened	One bolt loosened	Two bolts loosened	Three bolts loosened
Stiffness (N/m)	UKF predicted	2612.8	2597.1	2536.9	2497.7
	Calculated	2619.2	2608.3	2507.5	2470.2
Damping coefficient (N s/m)	UKF predicted	0.5744	1.1273	0.9616	1.0848
	Calculated	0.0894	0.1022	0.0992	0.1106

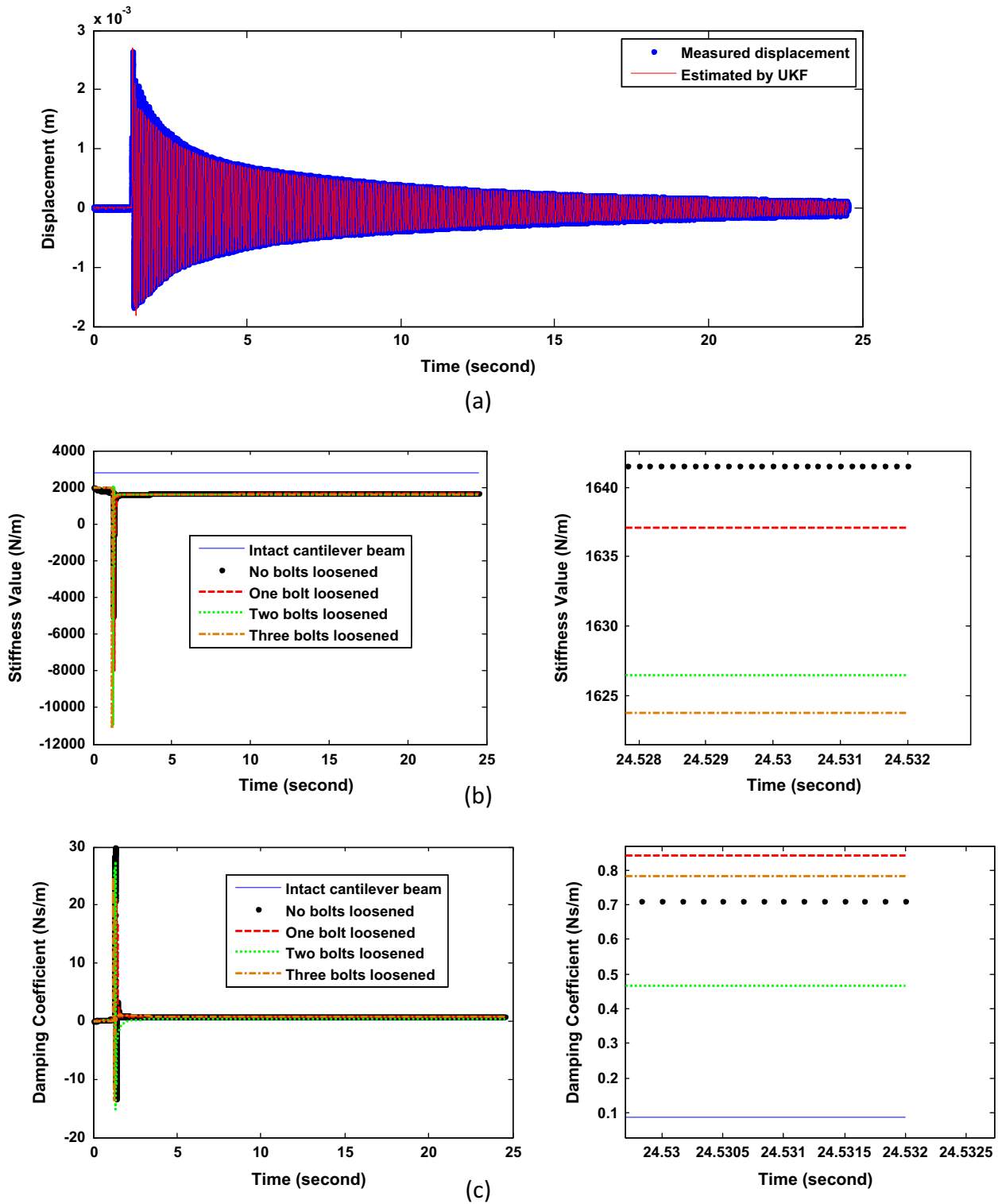


Fig. 9. Reduced section beam; (a) displacement comparison between measured by phase-based optical flow and predicted by UKF; (b) detailed view of predicted stiffness values of the section reduced beam with bolts loosened scenarios; (c) detailed view of predicted damping coefficients of the section reduced beam with bolts loosened scenarios.

Table 4
UKF predicted and calculated stiffness and damping coefficients for section reduced beam cases.

		No bolts loosened	One bolt loosened	Two bolts loosened	Three bolts loosened
Stiffness (N/m)	UKF predicted	1641.5	1637.1	1626.5	1623.6
	Calculated	1652.4	1651.3	1642.2	1635.4
Damping coefficient (N s/m)	UKF predicted	0.7090	0.8402	0.4648	0.7810
	Calculated	0.0763	0.0756	0.0735	0.0832

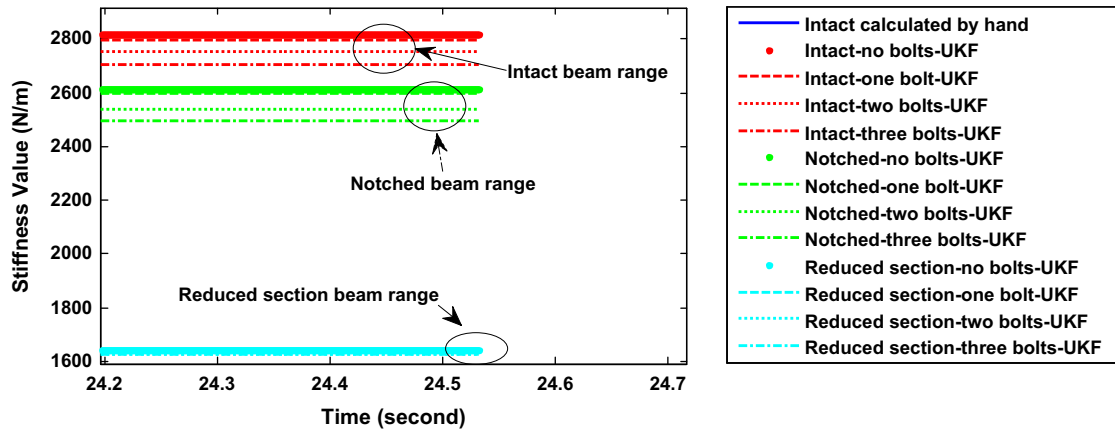


Fig. 10. Overall stiffness degradation due to various damage scenario cases of the cantilever beams.

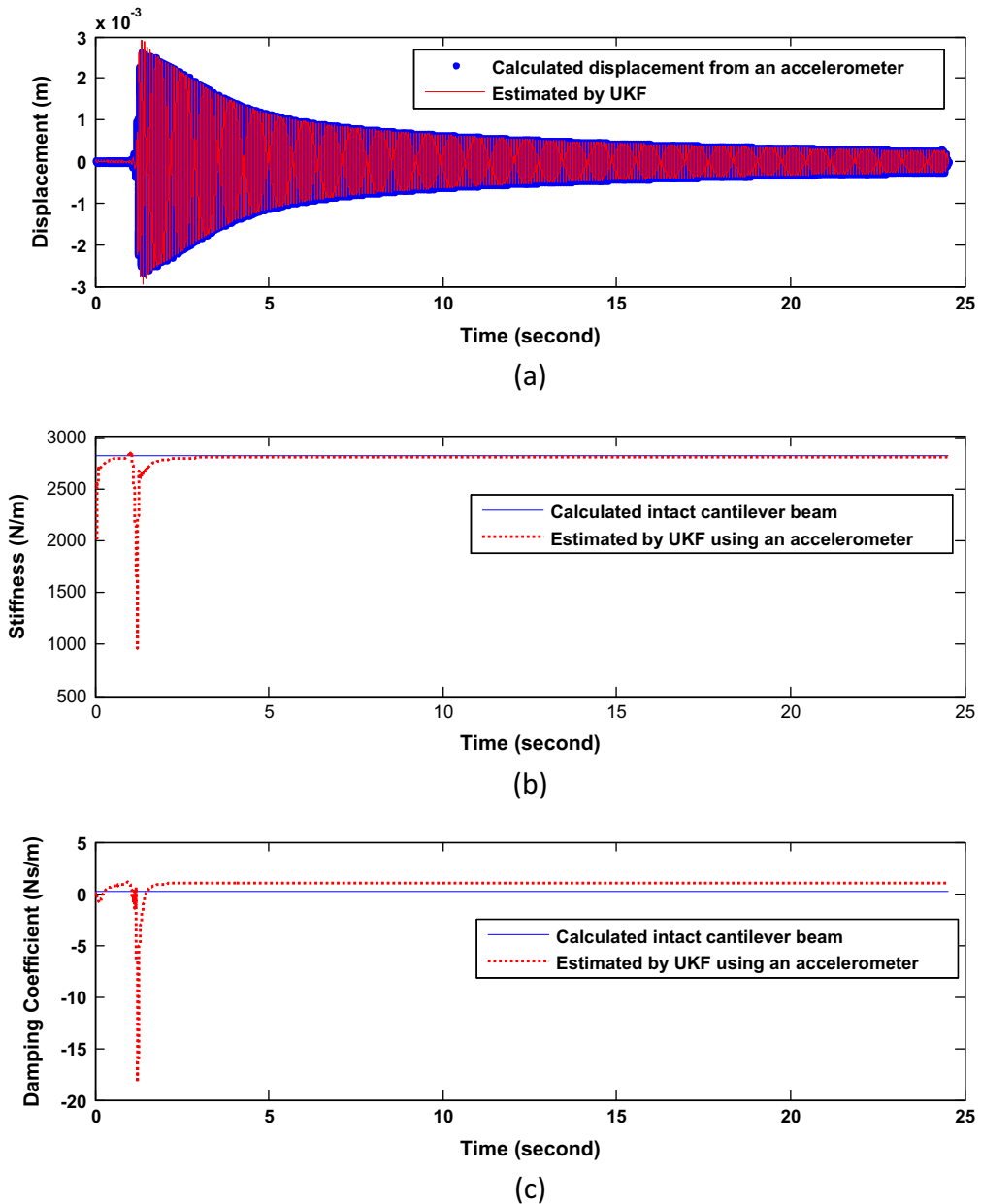


Fig. 11. Intact beam results using displacement achieved from an accelerometer; (a) displacement comparison; (b) predicted stiffness; (c) predicted damping coefficient.

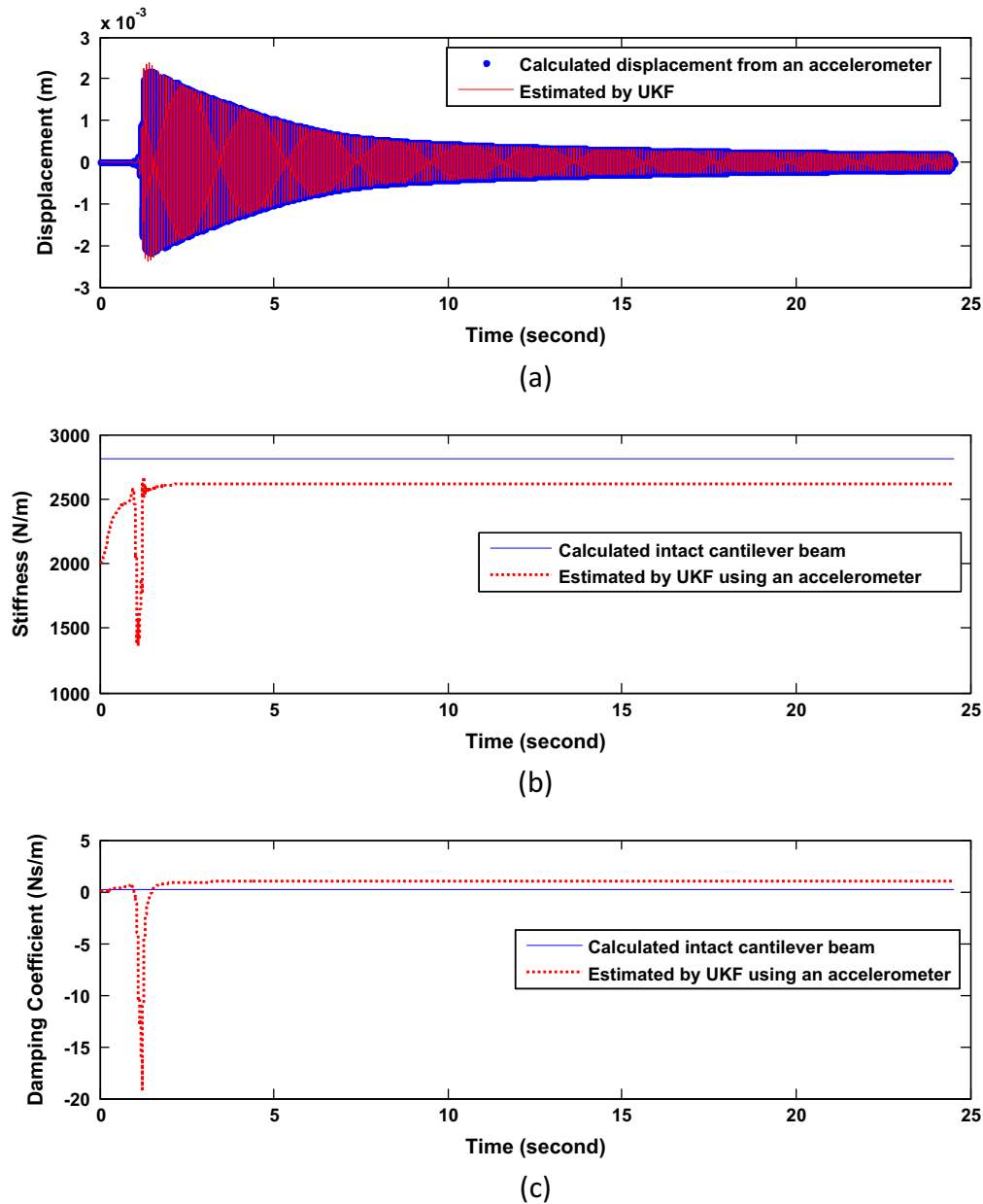


Fig. 12. Notched beam results using displacement achieved from an accelerometer; (a) displacement comparison; (b) predicted stiffness; (c) predicted damping coefficient.

cantilever beam with connection damage scenarios are reasonable compared to those of the intact beam cases. They show good agreement with similar discrepancies (i.e., approximately 1.2%) as in the case of the intact beam. The predicted damping coefficients are also reasonable when compared to the calculated values from the measured displacements. The predicted damping coefficient of the one-bolt loosened case deviates from the gradual increasing tendency relative to the increasing number of bolts loosened. However, this predicted value is still reasonable by checking measured values of the one-bolt loosened case.

4.3.3. Case 3: Section reduced cantilever beam

A section reduced cantilever beam as shown in Fig. 4 was investigated to examine major damage in the cantilever beam, and additionally the same bolt loosening connection damage scenarios were tested. Fig. 9(a) shows the reduction of stiffness due to the damage by reduced-section and the loosened bolts with a detailed view of the stiffness reductions. The predicted stiffness values are

gradually reduced due to reduction of the section of the beam and bolts loosening. Due to reduced section, the value of the stiffness is reduced from 2815.5 N/m to 1641.5 N/m which is approximately a 41% reduction. In order to validate the calculated stiffness based on dynamics and measured displacements, finite element analyses are carried out to calculate the equivalent stiffnesses using the commercial software ABAQUS [26]. The C3D10 (i.e., ten-node tetrahedral) elements are used in FE analyses, and the results show convergence with 3 mm mesh size in all cases. Applying a fixed condition to the left-end of the beams and a displacement to the right-end of the beams, equivalent stiffness is calculated using a force-displacement equation. The calculated stiffness for the Intact, Notched and Reduced section beams without loosened bolts are 2831.2, 2626.5 and 1655.5 N/m, respectively. As shown in Tables 2–4, the calculated stiffness using dynamics with the measured displacements are 2813.5, 2619.0, and 1652.4 N/m, respectively. This shows the stiffness calculated using dynamics was reasonable and predicted from the proposed UKF. Even though

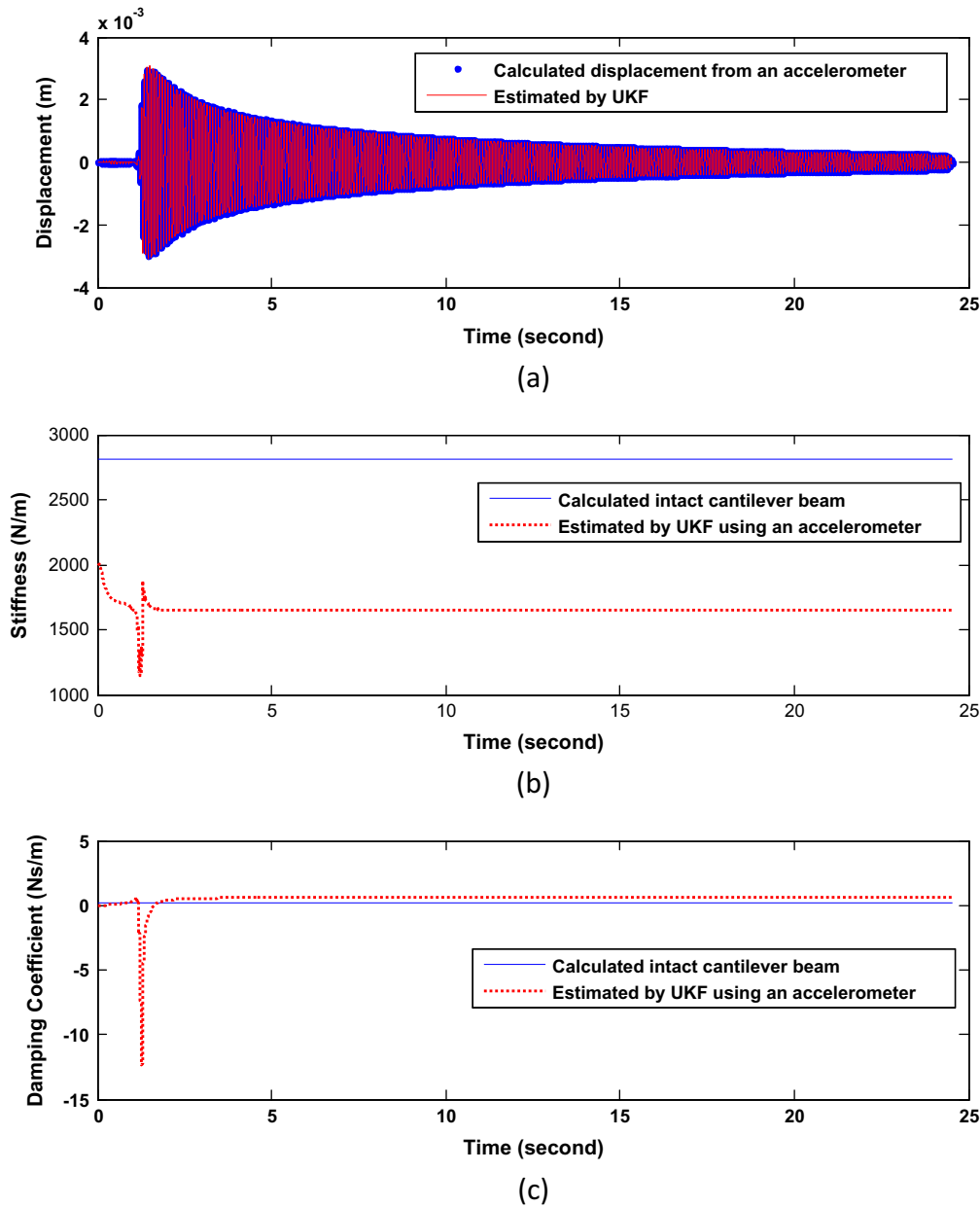


Fig. 13. Reduced-section beam results using displacement achieved from an accelerometer; (a) displacement comparison; (b) predicted stiffness; (c) predicted damping coefficient.

there is a heavy reduction of the stiffness due to section-reduced damage in the beam, the damping coefficients are relatively unchanged from those of the intact or notched beam cases as shown in Fig. 9(b) and Table 4.

The overall tendency of the reduction of the stiffness values due to small and major damage (i.e., notched damage and section reduced damage) and their bolts loosened connection damage scenarios is presented by plotting all predicted stiffness values of the previous three case studies, shown in different colors, in Fig. 10. Currently, as the system identifies a stiffness value for the system, identifying different types of damage using this methodology will be pursued as future work.

4.3.4. Comparative studies

In order to compare the results of the proposed method using video camera with different sensors, an accelerometer was installed atop the cantilever beam as shown in Fig. 3, used to

measure accelerations. The measured accelerations are twice integrated to obtain displacements for Intact, Notched, and Reduced-section beams without loosened bolts for comparative studies. Using the displacements, the stiffness and damping coefficients are predicted using the UKF. Fig. 11 shows the predicted displacement using UKF and obtained displacement using acceleration. Predicted stiffness and damping coefficient are also presented. The accelerometer measured and predicted displacements are slightly larger than those in Fig. 6 because the accelerometer is on top of the cantilever beam and the displacement from the video was calculated from beneath the accelerometer sensor. Thus, a larger displacement is reasonable to expect. The predicted stiffness and damping coefficient are 2806.6 N/m and 1.061 N s/m, respectively for the Intact cantilever beam. This is nearly identical to the 2815.5 N/m using the video camera and 2813.5 using hand calculations from the dynamics in Table 2. It is also similar to the equivalent stiffness (2831.2 N/m) within a 1% discrepancy from

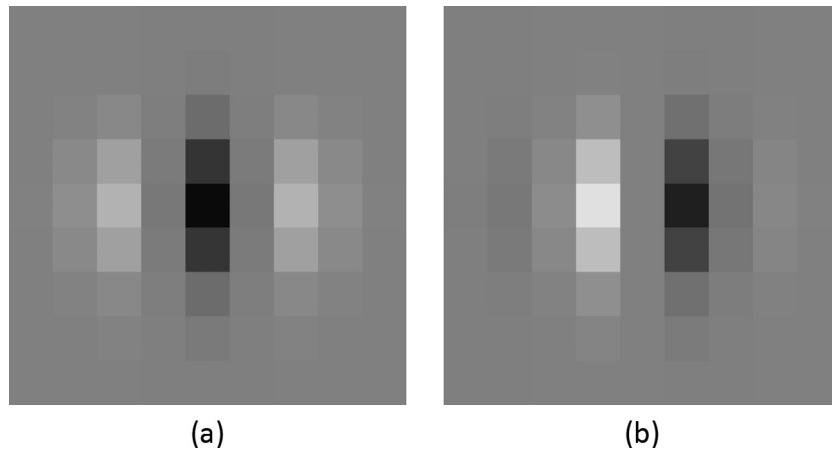


Fig. A1. Filters used to compute local phase and local amplitude: (a) real horizontal (G_2^0), (b) imaginary horizontal (H_2^0).

Table A1

Filter coefficients to compute horizontal and vertical local phase and local amplitude [18].

Tap #	G_{f1}	G_{f2}	H_{f1}	H_{f2}
−4	0.0094	0.0008	−0.0098	0.0008
−3	0.1148	0.0176	−0.0618	0.0176
−2	0.3964	0.1660	0.0998	0.1660
−1	−0.0601	0.6383	0.7551	0.6383
0	−0.9213	1.0000	0.0000	1.0000
1	−0.0601	0.6383	−0.7551	0.6383
2	0.3964	0.1660	−0.0998	0.1660
3	0.1148	0.0480	0.0618	0.0176
4	0.0094	0.0008	0.0098	0.0008
Filter				Filter in x
G_2^0 : Real horizontal				G_{f1}
H_2^0 : Imaginary horizontal				H_{f1}
$G_2^{\pi/2}$: Real vertical				G_{f2}
$H_2^{\pi/2}$: Imaginary vertical				H_{f2}

ABAQUS [26] from the previous section. In the case of the damping coefficient, the predicted value (1.061 N s/m) is much larger than the hand-calculated value (0.0871 N s/m) and the predicted value (0.4183 N s/m) using UKF from Table 2. However, this value is still reasonable because the critical damping ratio, ζ , calculated from $C = 2\zeta\sqrt{KM}$ is 0.0156, which is smaller than the 2% damping ratio for steel structures.

For the Notched beam, the predicted stiffness and damping coefficient using the achieved displacement obtained from the accelerometer are 2619.7 N/m, and 0.9869 N s/m, respectively. These values are also nearly identical to the values (2612.8 N/m; 0.5744 N s/m) predicted from UKF using video camera and values (2619.2 N/m; 0.0894 N s/m) calculated by hand using dynamics as shown in Table 3. Fig. 12 is presented for better understanding. The predicted stiffness and damping coefficient of the Reduced-section beam using the displacement achieved from the accelerometer's measurement are 1649.5 N/m and 0.5966 N s/m, respectively, as shown in Fig. 13. These values are also nearly identical to the values (1645.5 N/m; 0.7090 N s/m) predicted from UKF using video camera and values (1652.4 N/m; 0.0763 N s/m) calculated by hand using dynamics as shown in Table 4. As we found in the case of the Intact and Notched beam, the damping coefficient values are larger than those from video and hand calculation, but the values are still reasonable because the critical damping ratios, ζ , calculated from $C = 2\zeta\sqrt{KM}$ are 0.015 for the Notched beam and 0.0133 for the Reduced-section beam which are smaller than the 2% damping ratio for steel structures.

5. Conclusion

A novel damage detection methodology was proposed by integrating a computer vision based algorithm and the unscented Kalman filter (UKF). A video camera was used to record video to measure the displacement of the structural system at a select point of the system by processing via a computer vision algorithm, phase-based optical flow. As displacements measured from a video are quite accurate but have higher noise levels than traditional accelerometer measurements, the unscented Kalman filter was used to denoise the video measured displacement and detect damage by identifying structural properties such as stiffness and damping coefficient assuming a known mass of the structural system. Dynamic equations of motion to represent the behavior of the cantilever beam excited by an impact force were formulated to obtain state space equations without explicit excitation input for the UKF process, whereas in previous Kalman filtering approaches the input forces need to be explicitly known. The limitation of this approach is the complexity of the dynamic equation of motion. To apply it to large-scale structures subjected to ambient vibrations, simplified dynamic formulations are required, which will be included in future work.

The performance of the damage detection method was demonstrated through various experimental tests on a cantilever beam system. In order to investigate various damage types and a broad range of damage levels, beam damage types such as a manufactured notch, section reduction, and connection damage by loosening bolts were considered. The method accurately predicted the displacement by removing noise from the measured displacement for use with phase-based methods and video, and the video, and the method detected all these types of damage accurately by predicting structural properties and comparing to those of an intact beam. The predicted stiffness structural property showed a consistent tendency where it gradually decreased by the level of damage in terms of member damage and connection damage. There were no significant changes in the damping values between intact and damage scenarios. The predicted stiffness and damping coefficients were relatively accurate as compared to the calculated values from stiffness method using the member dimensions. Moreover, through comparative studies using an accelerometer, the predicted stiffnesses were compared and showed identical to the hand calculations, and those predicted stiffnesses were also validated by FE analyses using the commercial software ABAQUS. From these experimental investigations, the performance of the damage detection method using computer vision and UKF is demonstrated.

Acknowledgements

The authors acknowledge the support provided by Royal Dutch Shell through the MIT Energy Initiative, and thank chief scientists Dr. Dirk Smit and Dr. Sergio Kapusta, and project managers Dr. Lorna Ortiz-Soto and Dr. Keng Yap for their oversight of this work. We also acknowledge Draper Laboratory for providing experimental equipment.

Appendix A

See Fig. A1 and Table A1.

References

- [1] Cha YJ, Trocha P, Büyüköztürk O. Field measurement-based system identification and dynamic response prediction of a unique MIT building. *Sensors* 2016;16(7):1016.
- [2] Park JW, Lee JJ, Jung H, Myung H. Vision-based displacement measurement method for high-rise building structures using partitioning approach. *NDT and E Int* 2010;43(7):642–7.
- [3] Feng D, Feng MQ, Ozer E, Fukuda Y. A vision-based sensor for noncontact structural displacement measurement. *Sensors* 2015;15(7):16557–75.
- [4] Wahbeh AM, Caffrey JP, Masri SF. A vision-based approach for the direct measurement of displacements in vibrating systems. *Smart Mater Struct* 2003;12(5):785–94.
- [5] Lee JJ, Shinozuka M. Real-time displacement measurement of a flexible bridge using digital image processing techniques. *Exp Mech* 2006;46(1):105–14.
- [6] Chen J, Wadhwa N, Cha YJ, Durand F, Freeman W, Buyukozturk O. Structural modal identification through high speed camera video: motion magnification. *J Sound Vib* 2015;345:58–71.
- [7] Smyth AW, Masri SF, Chassiakos AG, Caughey TK. On-line parametric identification of MDOF nonlinear hysteretic systems. *J Eng Mech* 1999;125(2):133–42.
- [8] Smyth AW, Masri SF, Kosmatopoulos EB, Chassiakos AG, Caughey TK. Development of adaptive modeling techniques for non-linear hysteretic systems. *Int J Non-Linear Mech* 2002;37(8):1435–51.
- [9] Yang JN, Lin S. Identification of parametric variations of structures based on least squares estimation and adaptive tracking technique. *J Eng Mech* 2005;131(3):290–8.
- [10] Hoshiya M, Saito E. Structural identification by extended Kalman filter. *J Eng Mech* 1984;110(12):1757–70.
- [11] Yang JN, Lin S, Huang H, Zhou L. An adaptive extended Kalman filter for structural damage identification. *Struct Control Health Monit* 2006;13(4):849–67.
- [12] Julier SJ, Uhlmann JK, Durrant-Whyte HF. A new approach for filtering nonlinear systems. In: *Proceedings of the IEEE American control conference*, vol. 3; 1995. p. 1628–32.
- [13] Julier SJ, Uhlmann JK. Unscented filtering and nonlinear estimation. *Proc IEEE* 2004;92(3):401–22.
- [14] Wu M, Smyth AW. Application of the unscented Kalman filter for real-time nonlinear structural system identification. *Struct Control Health Monit* 2007;14(7):971–90.
- [15] Chatzi EN, Smyth AW. The unscented Kalman filter and particle filter methods for nonlinear structural system identification with non-collocated heterogeneous sensing. *Struct Control Health Monit* 2009;16(1):99–123.
- [16] Xie Z, Feng J. Real-time nonlinear structural system identification via iterated unscented Kalman filter. *Mech Syst Signal Process* 2012;28:309–22.
- [17] Bisht SS, Singh MP. An adaptive unscented Kalman filter for tracking sudden stiffness changes. *Mech Syst Signal Process* 2014;49(1):181–95.
- [18] Moireau P, Chapelle D. Reduced-order Unscented Kalman Filtering with application to parameter identification in large-dimensional systems. *ESAIM: Control, Optim Calculus Var* 2011;17(02):380–405.
- [19] Wadhwa N, Rubinstein M, Durand F, Freeman WT. Phase-based video motion processing. *ACM Trans Graphics (TOG)* 2013;2(4):80.
- [20] Freeman WT, Adelson EH. The design and use of steerable filters. *IEEE Trans Pattern Anal Mach Intell* 1991;13(9):891–906.
- [21] Fleet DJ, Jepson AD. Computation of component image velocity from local phase information. *Int J Comput Vision* 1990;5(1):77–104.
- [22] Gautama T, Van Hulle MM. A phase-based approach to the estimation of the optical flow field using spatial filtering. *IEEE Trans Neural Networks* 2002;13(5):1127–36.
- [23] Horn BK, Schunck BG. Determining optical flow. In: *Technical symposium east international society for optics and photonics*; 1981. p. 319–331.
- [24] Lucas BD, Kanade T. An iterative image registration technique with an application to stereo vision. *IJCAI* 1981;81:674–9.
- [25] <http://www.adept.net.au/cameras/visionresearch/Phantomv10.shtml>.
- [26] ABAQUS. 'ABAQUS Documentation', Dassault Systèmes, Providence, RI, USA; 2011.